Solar modulation of cosmic proton and helium with AMS-02

Bing-Bing Wang,[1] Xiao-Jun Bi,[2,3] Kun Fang,[2] Su-Jie Lin,[4] and Peng-Fei Yin[2]

[1]*Center for Space Plasma and Aeronomic Research (CSPAR), University of Alabama in Huntsville, Huntsville, Alabama 35899, USA*

[2]*Key Laboratory of Particle Astrophysics, Institute of High Energy Physics, Chinese Academy of Sciences, Beijing 100049, China*

[3]*School of Physical Sciences, University of Chinese Academy of Sciences, Beijing 100049, China*

[4]*School of Physics and Astronomy, Sun Yat-Sen University, Zhuhai, GuangDong 519082, China*

(Received 22 March 2022; accepted 26 August 2022; published 12 September 2022)

We investigate the solar modulation effect with the long-time cosmic ray (CR) proton and helium spectra measured by AMS-02 on the timescale of a Bartels rotation (27 days) between May 2011 and May 2017. The time covers the negative heliospheric magnetic field polarity cycle, the polarity reversal period, and the positive polarity cycle. The precise AMS-02 data provide an excellent opportunity to improve the understanding of the time-dependent solar modulation effect. In this work, a two-dimensional solar modulation model is used to compute the propagation of cosmic rays in the heliosphere. The CR propagation equation is numerically solved by the public code SOLARPROP. We find that the drift effect is suppressed during the high solar activity period for a long time but nearly recovered in the first half of 2017. The time-dependent rigidity dependence of the mean free path is critical to reproduce the observations during the polarity reversal period. We also confirm that protons and helium have the same diffusive mean free path. The future monthly AMS-02 and PAMELA data will further confirm the vital assumption about the universal mean free path for all species. The monthly antiproton data will be crucial to break the degeneracy between the diffusion and drift effect and determine the level of drift effect during different epochs.

DOI: 10.1103/PhysRevD.106.063006

I. INTRODUCTION

Galactic cosmic rays (CRs) are mainly generated in supernova remnants and then propagate in the interstellar medium. When CRs enter the heliosphere, the low energy spectrum changes relative to the local interstellar spectrum (LIS) due to the interaction with the solar wind and the embedded magnetic field [1,2] known as solar modulation. The solar modulation effect limits our understanding of low energy CRs outside the heliosphere. Therefore, the study of solar modulation is important for studying the source of CRs, dark matter indirect measurement, and the CR transport process in the Galaxy and heliosphere [3–16].

The recent experimental results from Voyager 1, PAMELA, and AMS-02 have achieved great breakthroughs that are useful to understand the solar modulation effect. Voyager 1 flew outside the heliosphere in August 2012 and directly measured the LIS from a few to hundreds MeV/nucleon [17–19]. PAMELA provided the monthly measurements of the proton spectrum from 2006 to 2014 [20,21], which shed light on some details of the solar modulation effect [22–28]. Recently, the AMS-02 Collaboration published the continuous proton and helium energy spectra between 2011 and 2017, covering three periods related to the magnetic field polarity [29]. Some important results have been obtained, such as confirming the velocity dependence of the CR diffusion coefficient, finding the increase of the slope of the perpendicular mean free path during the polarity reversal period for low rigidity particles, remarkable time dependence of the power-law index of the parallel mean free path, and the presence of time delay between solar activity and diffusion parameters [30–33].

In Ref. [28] (hereafter, Paper I), we built a modulation model to reproduce the long-time PAMELA proton measurements from July 2006 to February 2014 with only one or two free parameters. The modulation model describes the main physical processes of the CR propagation in the heliosphere, including diffusion, convection, drift, and adiabatic energy loss. Meanwhile, some of the main factors affecting the solar modulation are taken from the observations, such as the magnitude of the heliospheric magnetic field, the solar wind speed, and the tilt angle of the heliospheric current sheet (HCS). We also deliberated to keep the model as simple as possible by adopting minimal free parameters. The 2D modulation code SOLARPROP [34,35] was used to solve the CR propagation equation in the heliosphere and obtain the modulated spectra. We found that some features of the modulation processes during the polarity reversal period, such as the suppression of the drift effect and the time variation of the rigidity dependence of the mean free path, were very different

compared with other periods. Based on the model and findings in Paper I, we analyze the modulation effect with AMS-02 proton data separately in three periods related to the hemispherical magnetic field polarity in this work.

The paper is organized as follows. In Sec. II, we briefly introduce the modulation model and generate the LIS for the proton and helium, which is necessary for the following analyses. In Sec. III, we compute the time-varying modulated proton spectra and compare them to the observations of AMS-02. In Sec. IV, we check the assumption that the proton and helium have the same mean free path by reproducing the helium spectra with the modulation parameters for the proton. Finally, we give a summary in Sec. V.

II. SOLAR MODULATION MODEL

Several reviews have discussed the modulation processes in great detail, such as Refs. [1,2]. There are four major modulation mechanisms for CRs in the heliosphere: diffusion of the irregularities of the heliospheric magnetic field, convection by the outward solar wind, particle drift in the nonuniform heliospheric magnetic field, and adiabatic energy loss. The CR propagation process in the heliosphere can be described by the Parker equation [36]:

$$\frac{\partial f}{\partial t} = -(\vec{V}_{sw} + \vec{V}_{\rm drift}) \cdot \nabla f + \nabla \cdot [K^s \cdot \nabla f] + \frac{\nabla \cdot \vec{V}_{sw}}{3} \frac{\partial f}{\partial \ln p}, \quad (1)$$

where $f(\vec{r}, p, t)$ is the omnidirectional distribution function, $\vec{r}$ is the position in the heliocentric spherical coordinate system, p is the particle momentum, $\vec{V}_{sw}$ is the solar wind speed, $\vec{V}_{\rm drift}$ is the drift speed, and K^s is the symmetric part of the diffusion tensor. The differential intensity related to the distribution function is given by $I = p^2 f$.

It is customary to assume that the diffusion coefficient can be separated into spatial and rigidity components [2]. The common assumption about the rigidity part is that all particle species have a universal function of rigidity [37–42]. In Paper I, we adopted a linear rigidity dependence of the diffusion coefficient and reproduced the PAMELA monthly proton measurements from 2006 to 2012. During the polarity reversal period that was assumed between November 2012 and March 2014 in Paper I (based on Ref. [43]), a time-dependent rigidity dependence was necessary to explain the observations. In the present work, the parallel diffusion coefficient is adopted as the following form taking into account the finding in Paper I:

$$k_{\parallel} = \frac{1}{3} k \beta \left(\frac{R}{1\ \rm GV} \right)^{\delta} \frac{B_E}{B}, \quad (2)$$

where $k = 3.6 \times 10^{22}\ k_0\ \rm cm^2/s$ is a scale factor to model the time dependence of the diffusion coefficient, β is the particle speed in units of the speed of light, δ determines the rigidity dependence of the diffusion coefficient (by default $\delta = 1$), B_E is the heliospheric magnetic field strength near Earth, $B = B_0/r^2\sqrt{1+\tan\psi}$ is the heliospheric magnetic field strength at the particle position, and ψ is the angle between the magnetic field direction and its radial direction [44]. The standard Parker magnetic field model [44] is used in this work. We take the perpendicular diffusion coefficient to be $k_{\perp} = 0.02 k_{\parallel}$ according to the test particle simulation [45]. The diffusion coefficient is also often marked as $k_{\parallel/\perp} = \frac{1}{3} v \lambda_{\parallel/\perp}$, where v is the particle speed, and $\lambda_{\parallel}$ ($\lambda_{\perp}$) is called the parallel (perpendicular) mean free path.

The gradient and curvature drift speed is written as $V_{gc} = q \frac{\beta R}{3} \nabla \times \frac{\vec{B}}{B^2}$, where q is the charge of the particle [46]. We describe the HCS drift following Ref. [47], where a thick, symmetric transition region determined by the tilt angle is used to simulate a wavy neutral sheet. The HCS drift speed V_{ns}^w is given by

$$\vec{V}_{ns}^{w} = \begin{cases} \mathrm{sgn}(q) A \frac{v \theta_{\triangle} \cos(\alpha)}{6 \sin(\alpha + \theta_{\triangle})} \vec{e}_r, & \pi/2 - \alpha - \theta_{\triangle} < \theta < \pi/2 + \alpha + \theta_{\triangle}, \\ 0, & \text{else}, \end{cases} \quad (3)$$

where $\mathrm{sgn}(q)$ is the charge sign and $\theta_{\triangle} \approx \frac{2RV_{sw}}{B_0 \Omega \cos\alpha}$. When the polar solar magnetic field directs outward in the northern (southern) hemisphere and inward in the southern (northern) hemisphere, it is said that the Sun is in a positive (negative) polarity cycle marked as $A > 0$ ($A < 0$). The product $\mathrm{sgn}(q)A$ determines the drift direction. Taking into account the possible suppression of the drift effect, a scale factor k_d (by default $k_d = 1$) is introduced, and the drift velocity is described as $V_{\rm drift} = k_d(V_{gc} + V_{ns}^w)$ [48,49].

The solar wind speed and the magnitude of magnetic field near Earth are taken from Ref. [50]. The tilt angle of the HCS is obtained from Ref. [51] with the "new" model. These quantities are backward averaged over several months, which corresponds to the time of solar wind propagation from the Sun to the modulation boundary assumed as 100 AU. Both the measurement values and backward-time-averaged values are shown in Fig. 1. We note that although the measurements on the basis of about 27 days (blue lines) show large fluctuations, the backward-time-averaged values are very smooth. Since the observed cosmic rays sampled the average helioshperic environment, the large jumps in the diffusion parameters from month to month in some models are not expected [31,33]. A more detailed description of our model is given in Paper I and the references therein. A discussion about the possible modulation effect resulting from the merged interaction regions [52–54] is not included in this work.

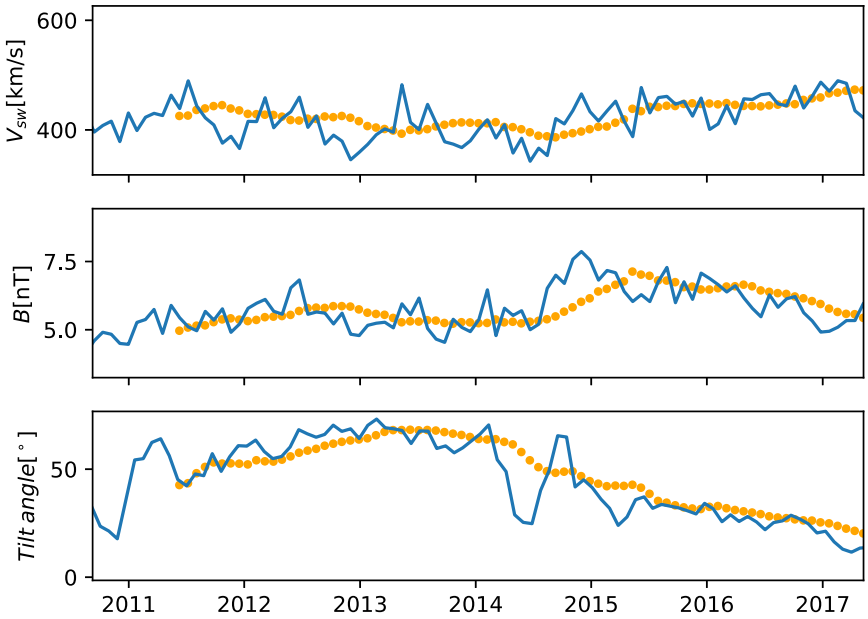

FIG. 1. Time profiles of the input interplanetary parameters in the solar modulation model. Panels from top to bottom: the solar wind speed, the magnetic field strength, and the tilt angle of the HCS. The blue lines indicate the measurements near Earth for each Carrington rotation. Orange dots represent the backward-time-averaged value, while orange dots in the top panel represent the backward time average for latitude-dependent solar wind speed minus 240 km/s.

As an initial input condition in the modulation model, the LIS is constrained by the current experimental measurements. Voyager 1 has directly measured the LIS in the range of a few to hundreds of MeV/nucleon. The monthly precise AMS-02 data provide important ingredients to reconstruct the LIS. The LIS for the proton and helium are constructed by the cubic spline interpolation method [7,28,55]. This method avoids the bias resulting from the CR injection and propagation models in the Galaxy that are still under debate. We match the low energy LIS to the Voyager 1 measurements and fit the calculated spectra to the AMS-02 data observed during the Bartels rotations 2429, 2432, 2435, and 2438 [19,29]. These periods are all within the negative polarity during which the data can be well explained by the modulation model with one free parameter k_0. The GNU Scientific Library [56] is used to perform the least-squares fitting. The energy knots and the corresponding intensities of the LISs are shown in Tables I and II for the proton and helium, respectively. Once the LISs are derived, the spectra at Earth can be directly predicted from the modulation model.

We show the LISs obtained in this work and those in Paper I in the top panel of Fig. 2. In Paper I, the proton (helium) LIS is obtained based on the Voyager 1 and PAMELA (BESS-POLARII) data. In the bottom panel, the ratios of the LIS to those in Paper I are shown. The differences of the LISs in the two papers are less than 5%.

III. SOLAR MODULATION FOR PROTONS

The AMS-02 data are taken during different solar activity levels and magnetic field conditions: the negative polarity cycle, the undefined polarity period around the solar maximum, and the positive polarity cycle. Paper I

TABLE I. The parametrization of the proton LIS with the cubic spline interpolation method. E_k is kinetic energy and I is intensity.

$\log(E_k/\mathrm{GeV})$	−2.42	−1.41	−0.50	0	0.50	1.00	1.50	2.00
$\log(I/\mathrm{GeV\,m^2\,sr\,s})$	4.2905	4.4688	4.0176	3.4548	2.5849	1.4158	0.0597	−1.3497

TABLE II. The parametrization of helium LIS with the cubic spline interpolation method. E_k is kinetic energy and I is intensity.

$\log(E_k/\mathrm{GeV})$	−2.27	−1.28	−0.30	0.56	1.22	1.78	2.29
$\log(I/\mathrm{GeV\,m^2\,s\,sr})$	2.3812	2.7324	2.6735	1.7705	0.4619	−0.8980	−2.2892

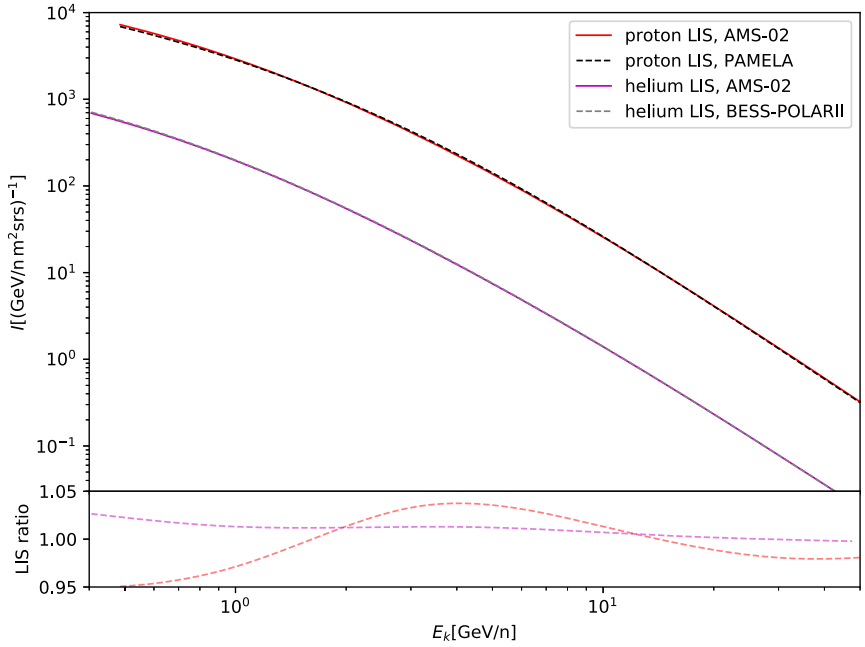

FIG. 2. The LISs of the proton and helium obtained in this work and those in Paper I. The ratios of the LISs to those in Paper I are shown in the bottom panel.

shows that the diffusion and drift processes differ between the negative and polarity reversal periods. Thus, we treat the modulation effect for the protons separately in three periods related to the heliospheric magnetic field polarity.

A. Modulation of the CR proton with the negative polarity assumption

The solar magnetic field reverses its polarity during every solar maximum. After the polarity reversal took place around 2000 [57], the polarity was negative until the recent reversal. As the cancellation of the opposite magnetic fluxes usually occurs first at lower latitudes, the polarity reversal at higher latitudes is later. Because of the asymmetric solar activity, the reversal of the solar magnetic field polarity is not simultaneous in the two hemispheres [58].

The solar magnetic field polarity reversal is observable. The analysis of the line-of-sight magnetic field data during 2010–2014 measured by the Helioseismic and Magnetic Imager on board the Solar Dynamic Observatory estimated that the northern and southern polar fields at latitude above 60° reversed in November 2012 and March 2014, respectively, and multiple reversals occurred in the north [43]. The analysis of the direct measurements of the solar magnetic field by the Vector Stokes Magnetograph on Synoptic Optical Long-term Investigations of the Sun found that the magnetic field in the southern hemisphere in the 60°–70° latitudinal range reversed its polarity in May 2013; at higher latitudes 65°–75°, the reversal occurred in November 2013 [59]. In the northern hemisphere at 60°–70°, the latitudinal range reversed its polarity in May 2012, March 2014, and February 2015; at latitudes 65°–75°, the reversals occurred in December 2012, May 2014, and March 2015 [59]. The measurements from the Wilcox Solar Observatory indicated that the polar magnetic field in the northern hemisphere at latitudes above 55° first reversed in May 2012 and completed the reversal in April 2014. In the southern hemisphere, the reversal first occurred in June 2013 and was completed in March 2015 [60]. The measurements of the solar magnetic fields above 55° from the magnetic database of the National Solar Observatory at Kitt Peak indicated that the reversal in the northern solar hemisphere occurred in June 2012 and was completed in November 2014; the reversal occurred in November 2013 in the southern hemisphere. A summary of some of the estimates of the solar polar field reversal times for the northern and southern solar hemispheres is presented in Table III.

One can see from Table III that the estimated reversal time can be very different based on different data and analysis. Some points about the complexity of the magnetic field reversal are worth emphasizing.

(1) The low latitude regions reverse their polarity earlier than the estimated time in Table III since these are based on observations for the high latitude magnetic field.
(2) The (partially) reversed solar magnetic field propagates outward by the solar wind. It takes time to result in the (partial) reversal of the heliospherical magnetic field. The heliospheric magnetic field polarity reversal is not only time dependent but also space dependent.
(3) The completion of the reversal of the heliospheric magnetic field is delayed compared with that of the

TABLE III. Estimates of the time of solar polar magnetic field polarity reversals in the northern and southern hemispheres.

North	South	Latitude	References
November 2012	March 2014	>60°	[43]
May 2012, March 2014, February 2015	May 2013	60°–70°	[59]
November 2012, May 2014, March 2015	November 2013	65°–75°	[59]
June 2012 to November 2014	November 2013	>55°	[61]
May 2012 to April 2014	June 2013 to March 2015	>55°	[60]

solar magnetic field, as the solar wind needs time to convect to the modulation boundary.

(4) Using the solar magnetic field polarity reversal time rather the completion of the hemispheric magnetic field polarity reversal time to determine the polarity ($A > 0$ or $A < 0$) is not appropriate.

(5) The polarity reversal process may cause the variation of turbulent hemispherical magnetic field (additional factors for these changes may also exist) and further change the cosmic ray diffusion coefficient.

While the polarity reversal period cannot be well determined, we can see that the solar polar magnetic field did not reverse before the early part of 2012. Thus, it is reasonable to set the heliospheric magnetic field polarity as negative before this time node. During the negative polarity cycle ($A < 0$), positively charged particles drifted into the inner heliosphere along the HCS and out over the poles.

We compare the computed spectra with the AMS-02 measurements with rigidity below 40 GV. For the particle with higher rigidity, the modulation effect is negligible. Following the scenario in Paper I that reproduces six years of PAMELA proton spectra between 2006 and 2012, we fix both k_d and δ as 1 and only adjust the scale factor of diffusion coefficient k_0 to fit the observations. Almost constant power-law indices are also observed in the double power-law diffusion coefficient model [32]. The resulting time profile of the reduced χ^2 [χ^2/(d.o.f.)] is shown in Fig. 3. The reduced χ^2 is around or less than 1 until August 2012. Thus, there is no significant need to introduce more free parameters for this period, which may introduce the risk of overfitting. The time profile of k_0 is summarized in Fig. 9 and is compatible with that of Paper I (see the comparison in Fig. 4). After August 2012, the reduced χ^2 increases to an unacceptable level with reduced $\chi^2 > 2$. The model with only one free parameter k_0 fails to correctly describe the modulation process and reproduce AMS-02 proton spectra after this time node. However, as shown in Paper I, this model could roughly provide an acceptable fit

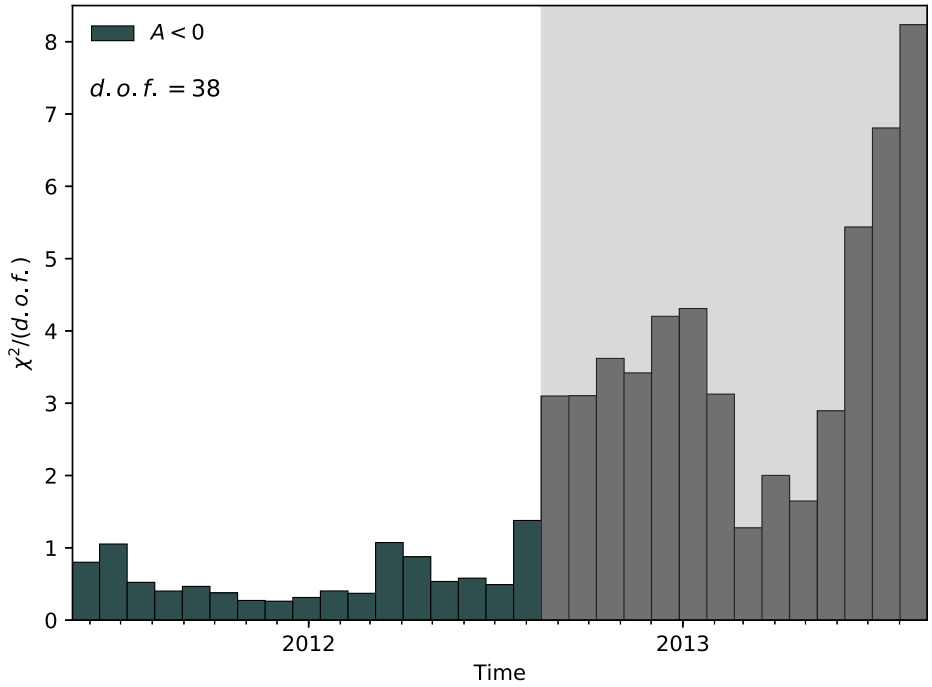

FIG. 3. The time profile of the reduced χ^2 for the fit to the monthly AMS-02 proton data from May 2011 to August 2012 under the assumption of $A < 0$. The scale factor of the diffusion coefficient k_0 is taken as the only free parameter.

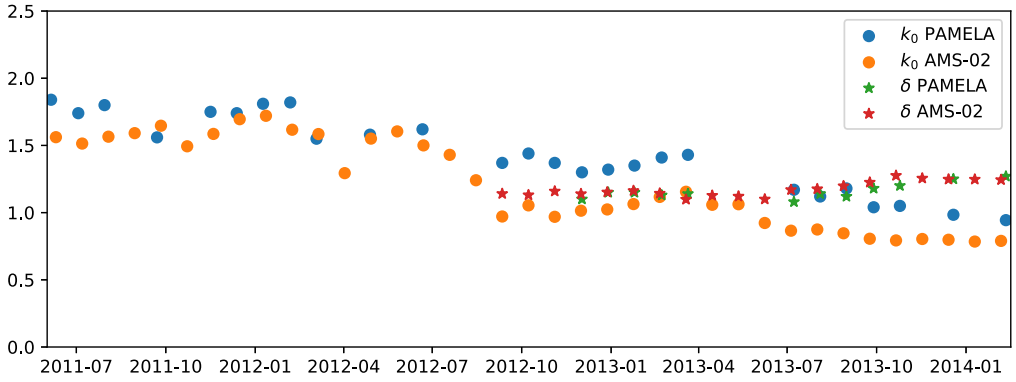

FIG. 4. Comparison between the best-fit parameters from Paper I and this work.

(not the best fit) to the PAMELA proton spectra between August 2012 and October 2013. The difference is due to the different spectra measured by two experiments.

In Fig. 4, we show a comparison between the best-fit parameters from Paper I for the PAMELA monthly proton data and this work for the AMS-02 proton data until August 2012 using the same modulation model. The two sets of parameters obviously show the same trend and are comparable with each other.

B. Modulation of CR proton with the positive polarity assumption

As shown in Table III, the estimated latest time of the completion of the solar polar magnetic field polarity reversal is March 2015 for some latitudes. The outward solar wind carries the reversed solar magnetic field into the heliosphere and finally results in the complete reversal of the heliospheric magnetic field polarity. Positively charged particles drift into the inner heliosphere over the poles and out of it along the HCS during the positive polarity cycle. They have less difficulty reaching Earth and less modulation than that during the negative polarity period.

When the solar activity recovers to a moderate or lower level, we expect the turbulent magnetic field properties and the resulting rigidity dependence of the mean free path to recover to behavior similar to that in the negative polarity cycle. We attempted to consider the full drift effect with $k_d = 1$ but found that the required scale factor of the diffusion coefficient k_0 was much smaller than 0.7 before October 2016 as shown in Fig. 5. Under the simple framework of the force-field approximation, the modulation potential is inversely proportional to the diffusion

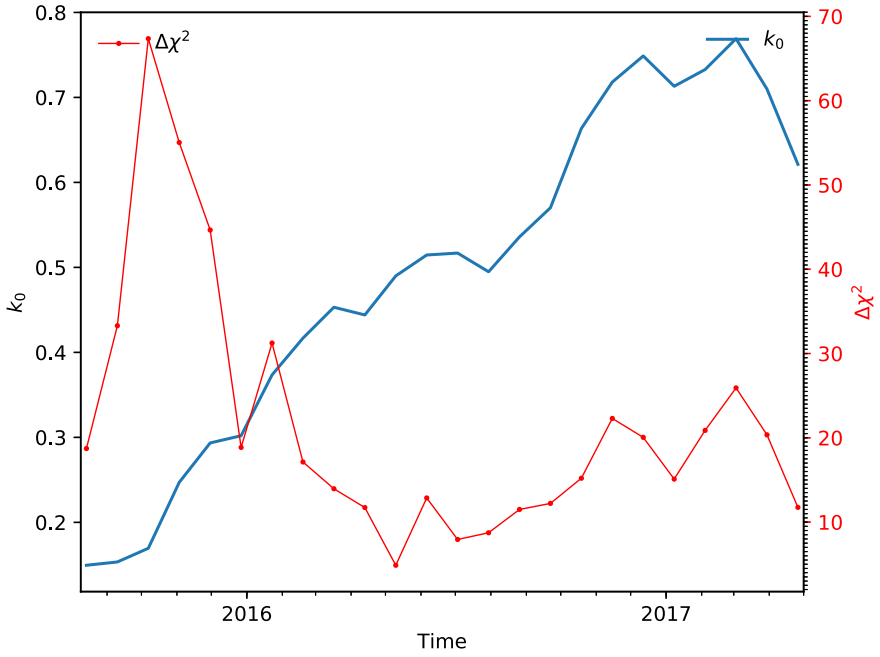

FIG. 5. The time profile of k_0 from April 2014 to May 2017 with the assumption of the positive polarity and the full drift effect. The χ^2 difference between the full and suppressed drift scenarios is marked as $\Delta\chi^2$.

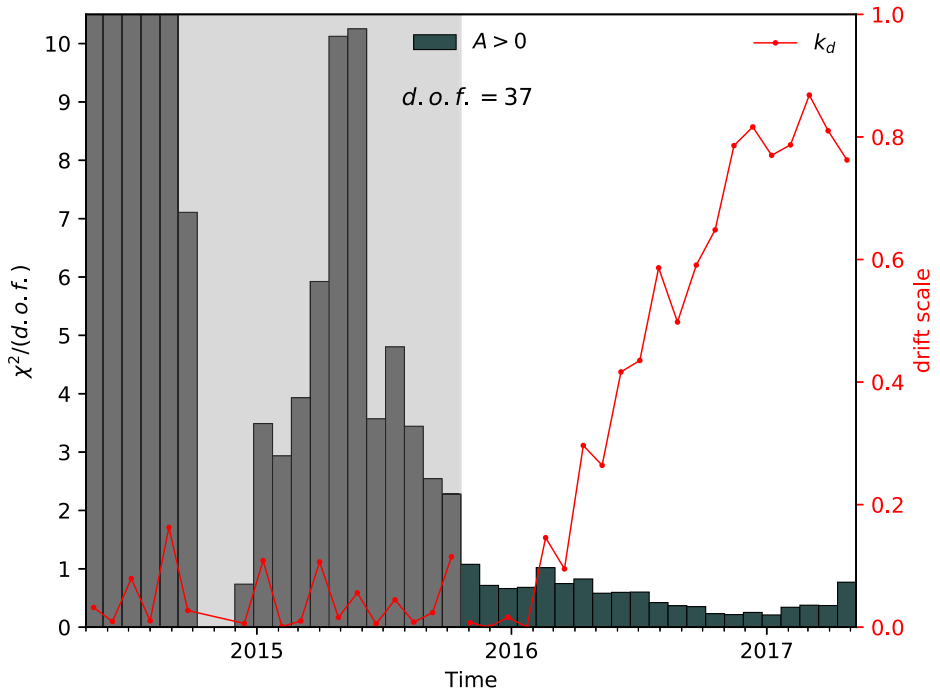

FIG. 6. The time profile of the reduced χ^2 and the drift scale factor k_d from the fits to the AMS-02 proton data from April 2014 to May 2017 under the assumption of $A > 0$. The scale factor for the diffusion coefficient and drift velocity k_0 and k_d are free parameters in this period.

coefficient characterized by k_0. Between May 2011 and May 2017, the ratio of the max value to the minimal value of the solar modulation potential reconstructed from the neutron monitor count rate is smaller than 2 [62,63]. If the full drift effect is adopted, the required diffusion coefficient would be too small and thus deviate from this result. In addition, this scenario results in a larger χ^2 than the drift suppressed model, as shown in Fig. 5. Consequently, we set k_d as a free parameter in this period to reduce the drift effect.

Figure 6 shows the time profile of the reduced χ^2 and the scale factor for the drift speed k_d between April 2014 and May 2017. The time profile of k_0 is summarized in the bottom panel of Fig. 9. The reduced-χ^2 values are only less than or close to 1 between November 2015 and May 2017. We also find that the reduced χ^2 is not acceptable before October 2015. The scale factor of drift velocity k_d is nearly 0 until the beginning of 2016 and increases to ~0.8 in March 2017. It indicates that the drift effect is suppressed during this period. The increase of k_d indicates the gradual recovery of the drift effect and implies that the drift effect may fully recover around the middle of 2017. Several mechanisms may cause the suppression of the drift effect. The large-scale fluctuations in the heliospheric magnetic field, such as the interaction regions and the merged interaction regions, fill the heliosphere so that drifts may only occur at a smaller scale during moderate to high solar activity periods [53]. In addition, numerical simulations show that the presence of scattering may also suppress the drift effect. For an intermediate degree of scattering, the drift velocity is typically suppressed by a large degree; when the scattering is very strong, there are no large-scale drift motions [64].

We note that there are strong degeneracies between k_0 and k_d and demonstrate an example in Fig. 7. k_0 and k_d are taken as input parameters here. The computed spectra are compared to the proton data taken from April 13, 2017 to May 9, 2017 in the positive polarity period. The red star

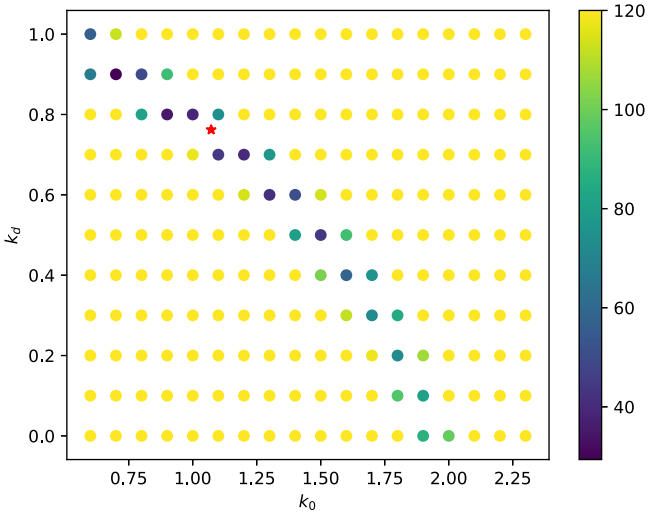

FIG. 7. The degeneracy between k_0 and k_d. The color indicates the reduced χ^2. The red star corresponds to the best fit with the reduced $\chi^2 = 0.76$.

indicates the best-fit values in the parameter space, while a few combinations for $k_d \in [0.5, 0.9]$ and $k_0 \in [0.75, 1.5]$ could also give a reasonable reduced χ^2. It can be seen that there is an obvious degeneracy between k_0 and k_d. A similar behavior could be found in Fig. 2 of Ref. [33]. Since the drift effect is opposite for particles with opposite charges, a simultaneous fit to the proton spectra and future monthly antiproton spectra is crucial to break the degeneracy and improve our understanding of the modulation process.

C. Modulation of the proton between August 2012 and October 2015

Section III A shows that the default model with the linear rigidity dependence on the mean free path and the full drift effect ($\delta = 1$ and $k_d = 1$) failed to describe the modulation process since August 2012. However, the model with linear rigidity dependence on the mean free path and the suppressed drift effect ($\delta = 1$ and $k_d \in [0, 1]$) used in Sec. III B cannot reproduce the observations before October 2015. In Paper I, we tested various configurations for the diffusion and drift effects to reproduce the PAMELA proton observations from November 2012 to February 2014 and concluded that the combination of the time-dependent rigidity dependence on the mean free path and the zero drift configuration gives the best fit to the data. Following Paper I, we introduce δ as an extra free parameter alongside k_0 to reproduce the AMS-02 observations between August 2012 and October 2015. This period covers some of the estimated solar magnetic field polarity reversal periods in Table III. Note that there is a coincidence between the variation of the power-law index of the mean free path and the estimated magnetic field reversal time. This may be a hint that the complex polarity reversal process induces the variation of the power spectrum of turbulence and the rigidity dependence of the mean free path. With such an assumption, we infer that the completion of heliospheric magnetic field polarity reversal may have occurred in the fourth quarter of 2015, and the completion of the solar magnetic field polarity reversal may have happened at the end of 2014 or beginning of 2015. The time profile of the slope of the mean free path δ and the reduced χ^2 are shown in Fig. 8. The time profile of k_0 is summarized in the bottom panel of Fig. 9. We find that δ roughly keeps increasing until it reaches the maximum value of 1.28 in October 2013 and then decreases to 1.07 in October 2015. The differences of δ between any two adjacent time nodes are smaller than 0.1. This agrees with our expectation that the diffusion parameters should be relatively smooth without large jumps from month to month. We also show a comparison between the best-fit parameters for the PAMELA and AMS data in the same periods after August 2012 in Fig. 4. We can see that these sets of parameters have the same trend and are comparable.

The variation of rigidity dependence should be noticed in all CR species, such as helium. Almost all the reduced χ^2's are smaller than 1. Therefore, the combination of the two free parameters k_0 and δ is adequate to reproduce the observations. Although introducing k_d as the third free

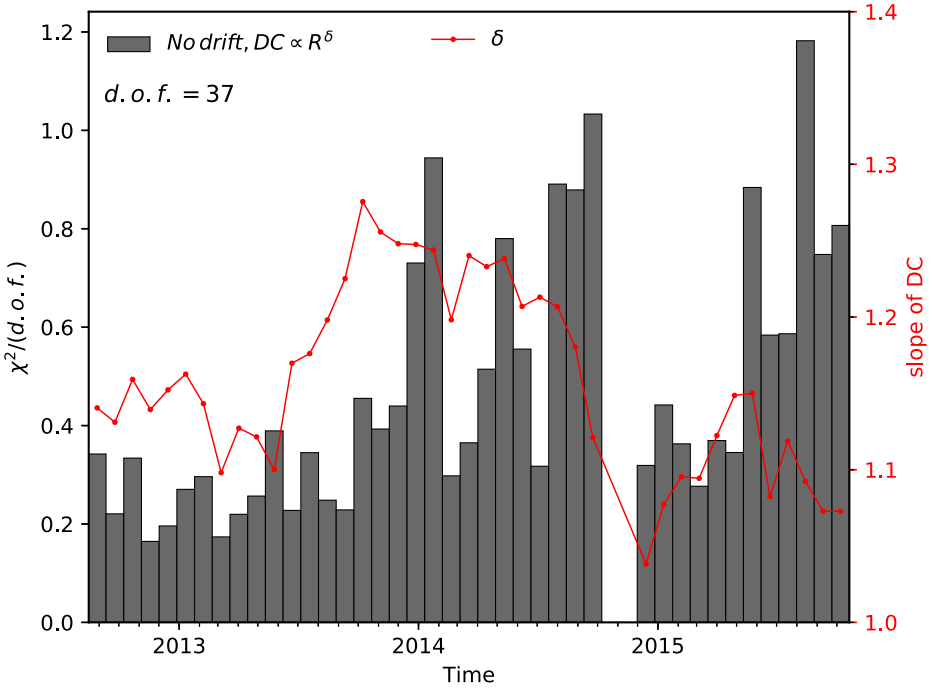

FIG. 8. Time profile of the reduced χ^2 and the slope of the mean free path δ for the fits to the AMS-02 proton data from August 2012 to October 2015. The scale factor for the diffusion coefficient k_0 and slope of the diffusion coefficient δ are free parameters in this period.

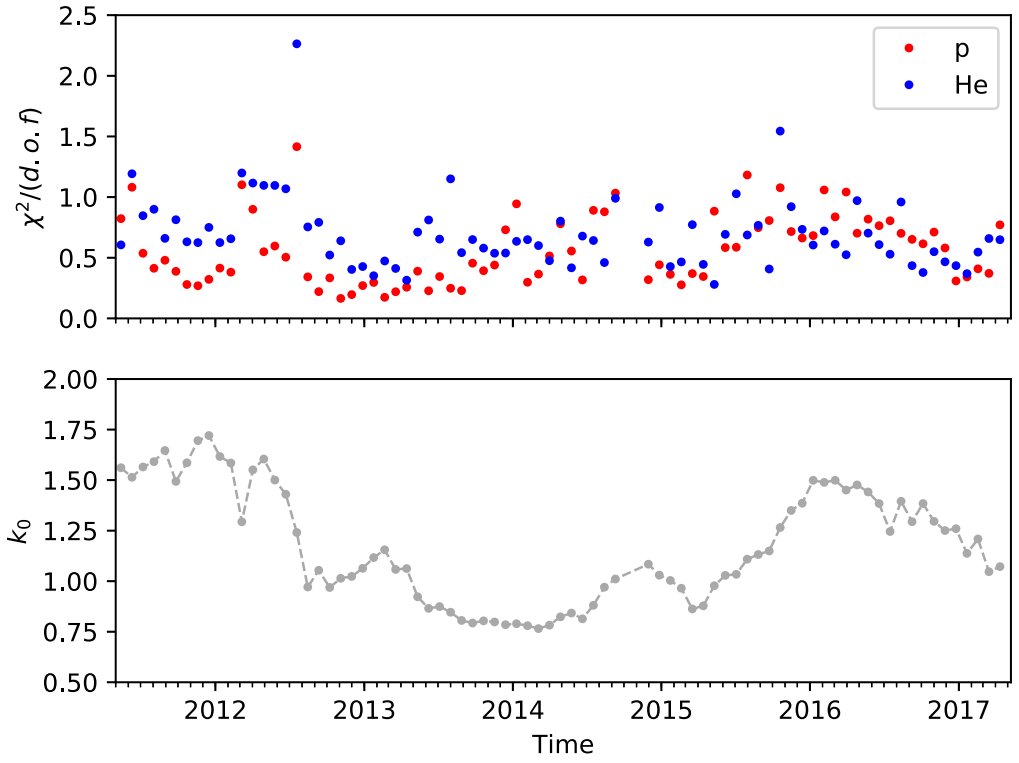

FIG. 9. The upper panel shows the time profile of the reduced χ^2 for the protons (red dots) and helium (blue dots). The bottom panel shows the best-fit k_0 for the protons. Note that in the upper panel, the modulation parameters for helium are taken from the fits to the proton data.

parameter may further improve the fit, the parameter space cannot be constrained well because of the degeneracy between the diffusion and drift parameters.

IV. SOLAR MODULATION FOR HELIUM

There is an important assumption that the mean free path is the same for all species of nuclei. The precise AMS-02 measurements provide a good opportunity to check this widely adopted assumption. The main parameter k_0 for the proton is shown in the bottom panel of Fig. 9. The time profiles of k_d and δ are shown in Figs. 6 and 8, respectively. We take the modulation parameters k_0, δ, and k_d obtained in the previous section as inputs to compute the modulated spectra for helium. The reduced χ^2's for helium and the proton are summarized in the upper panel of Fig. 9. We also show the ratios of the computed intensities to the measured intensities as functions of the rigidity and time in Fig. 10.

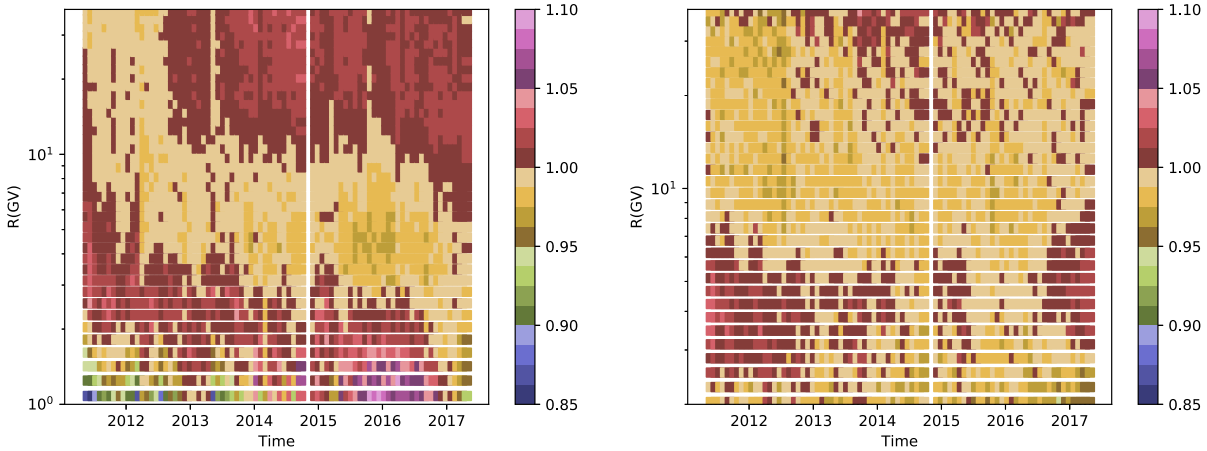

FIG. 10. The left (right) panel shows the ratio of the computed proton (helium) intensities to measured values. The same modulation parameters are applied for the proton and helium.

It can be seen that most of the fits agree with the data within ±5%. We find that the same modulation parameters can well reproduce the proton and helium observations simultaneously. This is consistent with some recent findings [30,31,33,65,66].

Recalling the treatment to the modulation for boron and carbon in Paper I, in which the same mean free paths can reproduce the ACE boron and carbon observations, different nuclei could have the same mean free path in the heliosphere. The future time-dependent nuclei data from AMS-02 and PAMELA will further check this assumption.

V. CONCLUSION

The precise AMS-02 measurements of the monthly CR proton and helium spectra between May 2011 and May 2017 provide an important chance to improve our understanding of the solar modulation effect. Compared to the PAMELA data up to February 2014, the AMS-02 data cover the whole solar magnetic field polarity reversal period around the solar maximum and part of the positive polarity cycle. Meanwhile, the precise measurements of the monthly helium spectrum provide a chance to check the important assumption that the CR proton and helium have the same diffusive mean free path in the heliosphere.

A two-dimensional solar modulation model is used to describe the propagation of protons and helium in the heliosphere. The model includes all major modulation processes and the variation of the heliosphere environment, such as the solar wind speed, the magnetic field strength, and the tilt angle of the HCS. The solar magnetic field polarity reversal period is not well determined from the direct observations. Furthermore, the time of magnetic field polarity reversal of the hemispherical magnetic field is different from that of the solar magnetic field. First, we investigate the modulation in a well-determined polarity period with the assumption that the mean free path is proportional to the particle rigidity. Then we investigate the modulation in the possible hemispheric magnetic field polarity reversal period. The simplest reasonable scenario is adopted to reproduce the observations. With no more than two free parameters and no risk of overfitting, the computed spectra can well reproduce the monthly AMS-02 proton and helium observations.

We find that the rigidity dependence of the mean free path varies with time. The linear rigidity dependence is adequate to reproduce the observations before August 2012 or after October 2015. In the possible polarity reversal period of hemispherical magnetic field between August 2012 and October 2015, the rigidity dependence of the mean free path $\propto R^{\delta}$ with a time varying δ is essential to fit the data. We also find that the zero drift effect can well reproduce the observations during this period, and the suppressed drift effect clearly keeps recovering. Finally, with the help of the precise monthly helium measurements, we confirm that the mean free path is the same for the proton and helium. The future monthly data of AMS-02 and PAMELA for other nuclei will further check the assumption that all the nuclei have a universal mean free path. In addition, the future monthly antiproton data would be invaluable to break the degeneracy between the diffusion and drift effect and understand the role of the drift effect in different solar activity periods.

ACKNOWLEDGMENTS

This work is supported by the National Key R&D Program of China (Grant No. 2016YFA0400200) and the National Natural Science Foundation of China (Grants No. U1738209 and No. 11851303).

[1] J. R. Jokipii, Propagation of cosmic rays in the solar wind, Rev. Geophys. Space Phys. **9**, 27 (1971).
[2] M. S. Potgieter, Solar modulation of cosmic rays, Living Rev. Solar Phys. **10**, 3 (2013).
[3] M. J. Boschini, S. Della Torre, M. Gervasi, D. Grandi, G. Jóhannesson, M. Kachelriess, G. La Vacca, N. Masi, I. V. Moskalenko, E. Orlando, S. S. Ostapchenko, S. Pensotti, T. A. Porter, L. Quadrani, P. G. Rancoita, D. Rozza, and M. Tacconi, Solution of heliospheric propagation: Unveiling the local interstellar spectra of cosmic-ray species, Astrophys. J. **840**, 115 (2017).
[4] Nicola Tomassetti, Solar modulation of galactic cosmic rays: Physics challenges for AMS-02, arXiv:1712.03178.
[5] M. J. Boschini, S. Della Torre, M. Gervasi, D. Grandi, G. Jóhannesson, G. La Vacca, N. Masi, I. V. Moskalenko, S. Pensotti, T. A. Porter, L. Quadrani, P. G. Rancoita, D. Rozza, and M. Tacconi, Deciphering the local interstellar spectra of primary cosmic-ray species with HELMOD, Astrophys. J. **858**, 61 (2018).
[6] M. J. Boschini, S. Della Torre, M. Gervasi, D. Grandi, G. Jóhannesson, G. La Vacca, N. Masi, I. V. Moskalenko, S. Pensotti, T. A. Porter, L. Quadrani, P. G. Rancoita, D. Rozza, and M. Tacconi, HelMod in the works: From direct observations to the local interstellar spectrum of cosmic-ray electrons, Astrophys. J. **854**, 94 (2018).
[7] Cheng-Rui Zhu, Qiang Yuan, and Da-Ming Wei, Studies on cosmic-ray nuclei with voyager, ACE, and AMS-02. I. Local interstellar spectra and solar modulation, Astrophys. J. **863**, 119 (2018).
[8] J. R. Jokipii, Radial variation of magnetic fluctuations and the cosmic-ray diffusion tensor in the solar wind, Astrophys. J. **182**, 585 (1973).

[9] A. Teufel and R. Schlickeiser, Analytic calculation of the parallel mean free path of heliospheric cosmic rays. I. Dynamical magnetic slab turbulence and random sweeping slab turbulence, Astron. Astrophys. **393**, 703 (2002).
[10] J. W. Bieber, Transport of charged particles in the heliosphere: Theory, Adv. Space Res. **32**, 549 (2003).
[11] J. W. Bieber, W. H. Matthaeus, A. Shalchi, and G. Qin, Nonlinear guiding center theory of perpendicular diffusion: General properties and comparison with observation, Geophys. Res. Lett. **31**, L10805 (2004).
[12] S. Parhi, J. W. Bieber, W. H. Matthaeus, and R. A. Burger, Heliospheric solar wind turbulence model with implications for *ab initio* modulation of cosmic rays, J. Geophys. Res. Space Phys. **109**, A01109 (2004).
[13] A. Shalchi, *Nonlinear Cosmic Ray Diffusion Theories*, Astrophysics and Space Science Library Vol. 362 (Springer Berlin, Heidelberg, 2009), 10.1007/978-3-642-00309-7.
[14] C. Pei, J. W. Bieber, B. Breech, R. A. Burger, J. Clem, and W. H. Matthaeus, Cosmic ray diffusion tensor throughout the heliosphere, J. Geophys. Res. Space Phys. **115**, A03103 (2010).
[15] L. L. Zhao, L. Adhikari, G. P. Zank, Q. Hu, and X. S. Feng, Influence of the solar cycle on turbulence properties and cosmic-ray diffusion, Astrophys. J. **856**, 94 (2018).
[16] Z. N. Shen and G. Qin, Modulation of galactic cosmic rays in the inner heliosphere over solar cycles, Astrophys. J. **854**, 137 (2018).
[17] E. C. Stone, A. C. Cummings, F. B. McDonald, B. C. Heikkila, N. Lal, and W. R. Webber, Voyager 1 observes low-energy galactic cosmic rays in a region depleted of heliospheric ions, Science **341**, 150 (2013).
[18] D. A. Gurnett, W. S. Kurth, L. F. Burlaga, and N. F. Ness, *In situ* observations of interstellar plasma with Voyager 1, Science **341**, 1489 (2013).
[19] A. C. Cummings, E. C. Stone, B. C. Heikkila, N. Lal, W. R. Webber, G. Jóhannesson, I. V. Moskalenko, E. Orlando, and T. A. Porter, Galactic cosmic rays in the local interstellar medium: Voyager 1 observations and model results, Astrophys. J. **831**, 18 (2016).
[20] O. Adriani *et al.*, Time dependence of the proton flux measured by PAMELA during the 2006 July-2009 December solar minimum, Astrophys. J. **765**, 91 (2013).
[21] M. Martucci *et al.*, Proton fluxes measured by the PAMELA experiment from the minimum to the maximum solar activity for solar cycle 24, Astrophys. J. Lett. **854**, L2 (2018).
[22] M. S. Potgieter, E. E. Vos, M. Boezio, N. De Simone, V. Di Felice, and V. Formato, Modulation of galactic protons in the heliosphere during the unusual solar minimum of 2006 to 2009, Sol. Phys. **289**, 391 (2014).
[23] Etienne E. Vos and Marius S. Potgieter, New modeling of galactic proton modulation during the minimum of solar cycle 23/24, Astrophys. J. **815**, 119 (2015).
[24] C. Corti, V. Bindi, C. Consolandi, and K. Whitman, Solar modulation of the local interstellar spectrum with Voyager 1, AMS-02, PAMELA, and BESS, Astrophys. J. **829**, 8 (2016).
[25] J. L. Raath, M. S. Potgieter, R. D. Strauss, and A. Kopp, The effects of magnetic field modifications on the solar modulation of cosmic rays with a SDE-based model, Adv. Space Res. **57**, 1965 (2016).
[26] N. Tomassetti, M. Orcinha, F. Barão, and B. Bertucci, Evidence for a time lag in solar modulation of galactic cosmic rays, Astrophys. J. Lett. **849**, L32 (2017).
[27] G. Qin and Z.-N. Shen, Modulation of galactic cosmic rays in the inner heliosphere, comparing with PAMELA measurements, Astrophys. J. **846**, 56 (2017).
[28] Bing-Bing Wang, Xiao-Jun Bi, Kun Fang, Su-Jie Lin, and Peng-Fei Yin, Time-dependent solar modulation of cosmic rays from solar minimum to solar maximum, Phys. Rev. D **100**, 063006 (2019).
[29] M. Aguilar *et al.*, Observation of Fine Time Structures in the Cosmic Proton and Helium Fluxes with the Alpha Magnetic Spectrometer on the International Space Station, Phys. Rev. Lett. **121**, 051101 (2018).
[30] N. Tomassetti, F. Barão, B. Bertucci, E. Fiandrini, J. L. Figueiredo, J. B. Lousada, and M. Orcinha, Testing Diffusion of Cosmic Rays in the Heliosphere with Proton and Helium Data from AMS, Phys. Rev. Lett. **121**, 251104 (2018).
[31] C. Corti, M. S. Potgieter, V. Bindi, C. Consolandi, C. Light, M. Palermo, and A. Popkow, Numerical modeling of galactic cosmic-ray proton and helium observed by AMS-02 during the solar maximum of solar cycle 24, Astrophys. J. **871**, 253 (2019).
[32] E. Fiandrini, N. Tomassetti, B. Bertucci, F. Donnini, M. Graziani, B. Khiali, and A. Reina Conde, Numerical modeling of cosmic rays in the heliosphere: Analysis of proton data from AMS-02 and PAMELA, Phys. Rev. D **104**, 023012 (2021).
[33] Xiaojian Song, Xi Luo, Marius S. Potgieter, XinMing Liu, and Zekun Geng, A numerical study of the solar modulation of galactic protons and helium from 2006 to 2017, Astrophys. J. Suppl. Ser. **257**, 48 (2021).
[34] http://www.th.physik.uni-bonn.de/nilles/people/kappl/.
[35] R. Kappl, SOLARPROP: Charge-sign dependent solar modulation for everyone, Comput. Phys. Commun. **207**, 386 (2016).
[36] E. N. Parker, The passage of energetic charged particles through interplanetary space, Planet. Space Sci. **13**, 9 (1965).
[37] L. J. Gleeson and I. H. Urch, Energy losses and modulation of galactic cosmic rays, Astrophys. Space Sci. **11**, 288 (1971).
[38] L. A. Fisk, Solar modulation of galactic cosmic rays, 2, J. Geophys. Res. **76**, 221 (1971).
[39] G. J. Fulks, Solar modulation of galactic cosmic ray electrons, protons, and alphas, J. Geophys. Res. **80**, 1701 (1975).
[40] H. Moraal, Cosmic-ray modulation equations, Space Sci. Rev. **176**, 299 (2013).
[41] M. J. Boschini, S. Della Torre, M. Gervasi, G. La Vacca, and P. G. Rancoita, Propagation of cosmic rays in heliosphere: The HELMOD model, Adv. Space Res. **62**, 2859 (2018).
[42] A. Vittino, C. Evoli, and D. Gaggero, Cosmic-ray transport in the heliosphere with HELIOPROP, Int. Cosmic Ray Conf. **35**, 24 (2017).
[43] X. Sun, J. T. Hoeksema, Y. Liu, and J. Zhao, On polar magnetic field reversal and surface flux transport during solar cycle 24, Astrophys. J. **798**, 114 (2015).
[44] E. N. Parker, Dynamics of the interplanetary gas and magnetic fields, Astrophys. J. **128**, 664 (1958).

[45] J. Giacalone and J. R. Jokipii, The transport of cosmic rays across a turbulent magnetic field, Astrophys. J. **520**, 204 (1999).
[46] J. R. Jokipii, E. H. Levy, and W. B. Hubbard, Effects of particle drift on cosmic-ray transport. I—General properties, application to solar modulation, Astrophys. J. **213**, 861 (1977).
[47] R. A. Burger and M. S. Potgieter, The calculation of neutral sheet drift in two-dimensional cosmic-ray modulation models, Astrophys. J. **339**, 501 (1989).
[48] S. E. S. Ferreira, M. S. Potgieter, and B. Heber, Particle drift effects on cosmic ray modulation during solar maximum, Adv. Space Res. **32**, 645 (2003).
[49] M. S. Potgieter, E. E. Vos, R. Munini, M. Boezio, and V. Di Felice, Modulation of galactic electrons in the heliosphere during the unusual solar minimum of 2006–2009: A modeling approach, Astrophys. J. **810**, 141 (2015).
[50] https://omniweb.gsfc.nasa.gov.
[51] https://wso.stanford.edu.
[52] M. S. Potgieter, J. A. Le Roux, L. F. Burlaga, and F. B. McDonald, The role of merged interaction regions and drafts in the heliospheric modulation of cosmic rays beyond 20 AU—A computer simulation, Astrophys. J. **403**, 760 (1993).
[53] M. S. Potgieter, Time-dependent cosmic-ray modulation—Role of drifts and interaction regions, Adv. Space Res. **13**, 239 (1993).
[54] Xi Luo, Marius S. Potgieter, Veronica Bindi, Ming Zhang, and Xueshang Feng, A numerical study of cosmic proton modulation using AMS-02 observations, Astrophys. J. **878**, 6 (2019).
[55] A. Ghelfi, F. Barao, L. Derome, and D. Maurin, Non-parametric determination of H and He interstellar fluxes from cosmic-ray data, Astron. Astrophys. **591**, A94 (2016).
[56] https://www.gnu.org/software/gsl/.
[57] N. Gopalswamy, A. Lara, S. Yashiro, and R. A. Howard, Coronal mass ejections and solar polarity reversal, Astrophys. J. Lett. **598**, L63 (2003).
[58] Y. M. Wang, N. R. Sheeley, and M. D. Andrews, Polarity reversal of the solar magnetic field during cycle 23, J. Geophys. Res. Space Phys. **107**, 1465 (2002).
[59] M. I. Pishkalo and U. M. Leiko, Dynamics of the circumpolar magnetic field of the Sun at a maximum of cycle 24, Kinematics and Physics of Celestial Bodies **32**, 78 (2016).
[60] Mykola I. Pishkalo, On polar magnetic field reversal in solar cycles 21, 22, 23, and 24, Sol. Phys. **294**, 137 (2019).
[61] P. Janardhan, K. Fujiki, M. Ingale, S. K. Bisoi, and D. Rout, Solar cycle 24: An unusual polar field reversal, Astron. Astrophys. **618**, A148 (2018).
[62] A. Ghelfi, D. Maurin, A. Cheminet, L. Derome, G. Hubert, and F. Melot, Neutron monitors and muon detectors for solar modulation studies: 2.ϕ time series, Adv. Space Res. **60**, 833 (2017).
[63] Sergey A. Koldobskiy, Veronica Bindi, Claudio Corti, Gennady A. Kovaltsov, and Ilya G. Usoskin, Validation of the neutron monitor yield function using data from AMS-02 experiment, 2011–2017, J. Geophys. Res. Space Phys. **124**, 2367 (2019).
[64] J. Minnie, J. W. Bieber, W. H. Matthaeus, and R. A. Burger, Suppression of particle drifts by turbulence, Astrophys. J. **670**, 1149 (2007).
[65] Nicola Tomassetti, Fernando Barão, Bruna Bertucci, Emanuele Fiandrini, and Miguel Orcinha, Numerical modeling of cosmic-ray transport in the heliosphere and interpretation of the proton-to-helium ratio in solar cycle 24, Adv. Space Res. **64**, 2477 (2019).
[66] M. D. Ngobeni, O. P. M. Aslam, D. Bisschoff, M. S. Potgieter, D. C. Ndiitwani, M. Boezio, N. Marcelli, R. Munini, V. V. Mikhailov, and S. A. Koldobskiy, The 3D numerical modeling of the solar modulation of galactic protons and helium nuclei related to observations by PAMELA between 2006 and 2009, Astrophys. Space Sci. **365**, 182 (2020).